ACS Catalysis

Research Article

pubs.acs.org/acscatalysis

DFT Study of Furfural Conversion to Furan, Furfuryl Alcohol, and 2-Methylfuran on Pd(111)

Vassili Vorotnikov,[†] Giannis Mpourmpakis,[†] and Dionisios G. Vlachos*[,†]

Department of Chemical and Biomolecular Engineering Catalysis Center for Energy Innovation and Center for Catalytic Science and Technology, University of Delaware, Newark, Delaware 19716, United States

Supporting Information

ABSTRACT: Dispersion-corrected density functional theory calculations were performed to investigate the adsorption of furan, furfural, furfuryl alcohol, and 2-methylfuran as well as the reaction barriers for their interconversion. The most stable configuration for furan, furfural, furfuryl alcohol, and 2-methylfuran entails the furan ring lying flat on the surface, centered over a hollow site. We performed an elementary step analysis for the reaction of furfural to furan, furfuryl alcohol, and 2-methylfuran. Thermodynamics favors the production of furan and CO. The activation energy for furfural reduction to furfuryl alcohol is lower than that for its decarbonylation to furan. The formation of 2-methylfuran occurs via dehydration of furfuryl alcohol or a dehydrogenation pathway through a methoxy intermediate. Our findings are in agreement with recently reported experimental results.

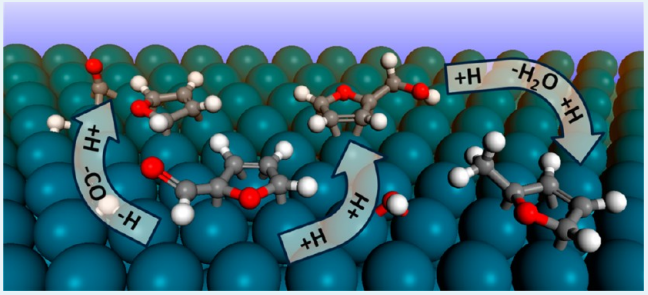

KEYWORDS: *furfural, furfuryl alcohol, furan, 2-methylfuran, Pd, DFT, PBE-D3, selective hydrogenation, hydrodeoxygenation*

1. INTRODUCTION

With increasing interest in renewable fuels, fuel additives, and chemicals, considerable attention has recently shifted toward biomass-derived building block molecules, such as 2,5-furandicarboxylic acid and furfural.[1] Hydrogenation products of these building blocks include 2-methylfuran, 2,5-dimethylfuran, tetrahydrofuran, 2-methyltetrahydrofuran, and furfuryl alcohol. Dimethylfuran, 2-methylfuran, 2-methyltetrahydrofuran, and furfuryl alcohol are potential fuels and fuel additives, and tetrahydrofuran is used as a solvent.[2] The selective hydrogenation of furfural to 2-methylfuran is of particular interest, since 2-methylfuran is a better additive to gasoline than 2-methyltetrahydrofuran.[2]

Palladium has been successfully used in low-temperature, aqueous-phase selective hydrogenation of furfural and hydroxymethylfurfural to methylfuran and dimethylfuran, respectively;[2,3] however, at higher temperatures, furfural undergoes decarbonylation to form furan and CO.[4] Since furfural can undergo either hydrogenation or decarbonylation on Pd, selectivity is important, and the mechanistic details gained by studying these reactions may be useful in designing cheaper, more active, and selective catalysts.

Since the first efforts in the catalytic upgrade of furfural,[5] it has been determined that the products of furfural chemical transformations on transition metal catalysts highly depend on the reactants' affinity to that metal. In addition, furfural is a multifunctional molecule and can potentially bind to a catalytic surface through its aromatic furan ring or through the carbonyl functional group. As a result, furfural can undergo decarbonylation on strong-binding Pd catalyst, on which "flat" adsorption through the furan ring is anticipated.[4,6,7] On the other hand, furfural undergoes hydrogenation to furfuryl alcohol and 2-methylfuran on the weaker-binding Cu catalyst,[8] on which adsorption through the carbonyl is expected.[9]

The adsorption geometry of furan and furfural has been theoretically investigated using the generalized gradient approximation (GGA) within the density functional theory (DFT).[7,9−14] Resasco, Balbuena, and co-workers utilized the PBE functional to complement kinetic studies of furfural hydrogenation.[7,9,12] Woodruff and co-workers used both the RPBE and the PW91 to analyze furan adsorption combined with near edge X-ray absorption fine structure and photoelectron diffraction experiments.[10,14] Medlin and co-workers used the PW91 functional to support temperature-programmed desorption (TPD) and reaction (TPR) experiments.[13]

Traditional GGA functionals sometimes fail to describe the interactions between aromatic molecules and metals as well as their adsorption geometries. Group 11 transition metals are particularly prone to these problems.[15] This inaccuracy arises from the GGA functionals' inability to account for the van der Waals (vdW) interactions,[16] since only the electrostatic forces are accounted for.[17,18] Because of this shortcoming of the standard DFT methods, we expect an inherent inaccuracy in first-principles catalyst design predictions. The greatest inaccuracies arise in weakly bound systems (less than ∼1

Received: June 19, 2012
Revised: September 2, 2012
Published: October 19, 2012

   dx.doi.org/10.1021/cs300395a | ACS Catal. 2012, 2, 2496−2504

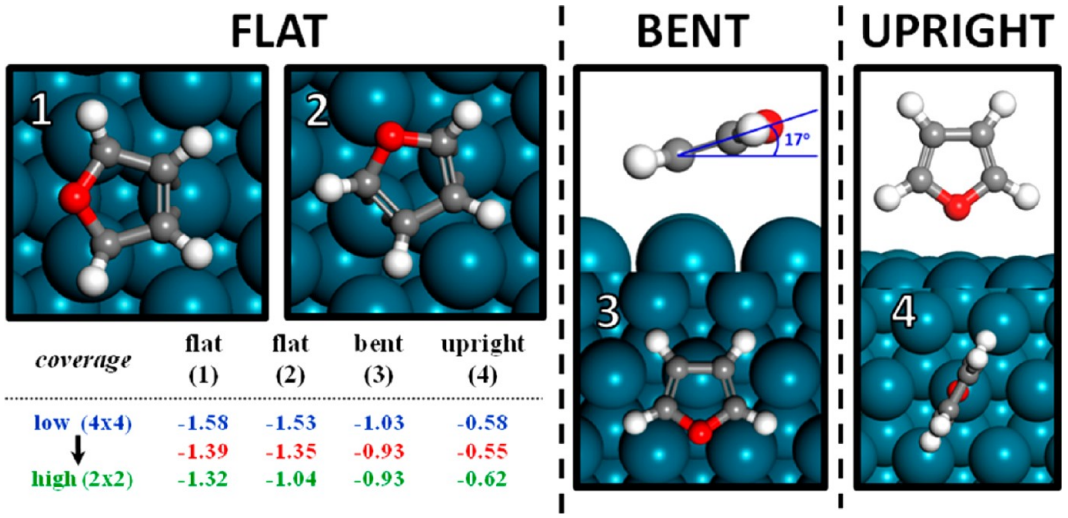

coverage	flat (1)	flat (2)	bent (3)	upright (4)
low (4x4)	-1.58	-1.53	-1.03	-0.58
↓	-1.39	-1.35	-0.93	-0.55
high (2x2)	-1.32	-1.04	-0.93	-0.62

Figure 1. Furan adsorption configurations on Pd(111): (1) flat, over fcc hollow site bound to 3 Pd atoms; (2) flat, over fcc hollow site bound to 2 Pd atoms; (3) bent, above the atop site; and (4) upright, above the atop site. The numbers (left) correspond to the adsorption energies (in eV) from top to bottom using: 4 × 4 (blue), 3 × 3 (red), and 2 × 2 (green).

eV), in which a mixture of electrostatic and vdW forces is expected.[19]

In this work, we use DFT methods that account for dispersive forces to calculate the energetics of furfural conversion to furan, furfuryl alcohol, and 2-methylfuran on Pd(111). To the best of our knowledge, this is the first theoretical study presenting both thermodynamics and kinetic barriers of furfural transformations on Pd.

2. METHODS

Bradley et al. calculated the adsorption energy of furan on Pd(111) at 0.45 eV using the RPBE functional,[10] underestimating the experimental values of 1.03 ± 0.26 eV and 0.94 ± 0.19 eV obtained from laser-induced thermal desorption[10] and TPD experiments,[20] respectively. The adsorption energies of 1.11 and 0.97 eV, using PW91 and PBE functionals, respectively, are in close agreement with the experiments, but for the *wrong reasons*, as concluded by Woodruff and coworkers.[10,17] These authors state that it is the exchange part of the functional that is responsible for this phenomenon. Nonlocal dispersive forces, which are not accounted for in the standard GGA functionals, are responsible for the underestimation of binding using the RPBE functional. This also implies that the PBE and PW91 performance with respect to such interactions is merely a coincidence.

The effect of nonlocal interactions is pronounced in the case of thiophene, a molecule similar to furan. Thiophene has been probed both experimentally and theoretically on different surfaces of copper, a metal used in furfural upgrade to furfuryl alcohol and 2-methylfuran.[4,6,7,9] Sony et al. studied thiophene on Cu(110) using vdW density functional (vdW-DF) and showed that vdW interactions are the governing forces in the adsorption process. Without the inclusion of nonlocal correlation energy, the RPBE predicted no adsorption at all, which is clearly inconsistent with the experiments.[21] A study of thiophene on Cu(111) using the DFT-D method to account for vdW interactions yielded a much closer structural and energetic agreement with the experiment than the standard PBE and PW91 functionals.[17]

Here, we carried out plane-wave DFT calculations using the Vienna Ab Initio Simulation Package (VASP), version 5.2.12.[22,23] The electron−electron exchange and correlation energies were computed using the Perdew, Burke, and Ernzerhof functional with the latest dispersion correction, PBE-D3.[24,25] For comparison, we also used the standard PBE functional. The projector augmented-wave method was used for the electron−ion interactions.[26,27] We used a plane-wave basis set with an energy cutoff of 400 eV.

For bulk calculations, a tetrahedron method with Blochl corrections and 15 × 15 × 15 Monkhorst−Pack *k*-point mesh was used.[28,29] The bulk lattice constant was obtained using the Birch−Murnaghan equation of state.[30,31] The Pd fcc lattice constant was calculated to be 3.95 Å using the PBE and 3.90 Å using the PBE-D3, both of which are in good agreement with the experimental value of 3.89 Å.[32] For benchmarking purposes, we carried calculations for thiophene on Cu (Supporting Information). The Cu fcc lattice constant was calculated to be 3.64 Å using PBE and 3.57 Å using the PBE-D3, again both in good agreement with the experimental value of 3.61 Å.[33]

The metal slab was modeled with a 4 × 4, a 3 × 3, or a 2 × 2 unit cell composed of four atomic layers. The bottom two layers were frozen. The 4 × 4 unit cell was used in all calculations to minimize adsorbate interaction effect. The 3 × 3 and the 2 × 2 unit cells were used in exploring the coverage dependence in the adsorption of furan. The vacuum between the slabs was set at 20 Å to minimize the effect of the slab. The Brillouin zone was sampled with a 3 × 3 × 1, 5 × 5 × 1, and 9 × 9 × 1 *k*-point grid for 4 × 4, 3 × 3, and 2 × 2 unit cells, respectively. For accurate total energies, we used the Methfessel−Paxton method with a smearing parameter of 0.1. An RMM-DIIS quasi-Newton algorithm was used in the energy minimization.[34] Surface relaxation was performed until all forces were smaller than 0.05 eV/Å. For selected structures, further surface relaxation was performed until all forces were smaller than 0.02 eV/Å, but no significant change in the adsorbate conformation or total energy was observed.

The adsorption energy was computed as $\Delta E_{ads} = E_{slab+i} - E_{slab} - E_i$, where E_{slab+i} is the total electronic energy of the metal slab−adsorbate system, E_{slab} is the total electronic energy of a clean slab, and E_i is the total electronic energy of the adsorbate in the gas phase. The supercell for all gas-phase calculations was chosen to be 20 × 21 × 22 Å. We performed tests for energy

dx.doi.org/10.1021/cs300395a | ACS Catal. 2012, 2, 2496−2504

Table 1. Properties of Furan Adsorption on Pd(111) and Comparison to Experiments[a]

	$d_{Pd-\alpha C}$ (Å)	$d_{Pd-\beta C}$ (Å)	d_{Pd-O} (Å)	ΔE_{ads} (eV)	E_{disp} (eV)
RPBE (3 × 3 unit cell)[10]	2.11	2.23	2.81	−0.45	
PBE (3 × 3 unit cell)	2.11	2.22	2.81	−0.97	
PBE-D3 (4 × 4 unit cell)	2.13	2.21	2.80	−1.58	−0.73
PBE-D3 (3 × 3 unit cell)	2.13	2.20	2.81	−1.39	−0.73
PBE-D3 (2 × 2 unit cell)	2.09	2.21	2.82	−1.32	−1.14
experiments[14]	2.13 ± 0.03	2.34 ± 0.13	2.42 ± 0.08	−1.03 ± 0.26[10]	
				−0.94 ± 0.19[20]	

[a]The distances are from the nearest Pd atom to (a) the carbon atom closest to the oxygen, $d_{Pd-\alpha C}$; (b) the carbon atom farthest from the oxygen, $d_{Pd-\beta C}$; and (c) the oxygen, d_{Pd-O}. E_{disp} represents the computed van der Waals contribution to the adsorption energy.

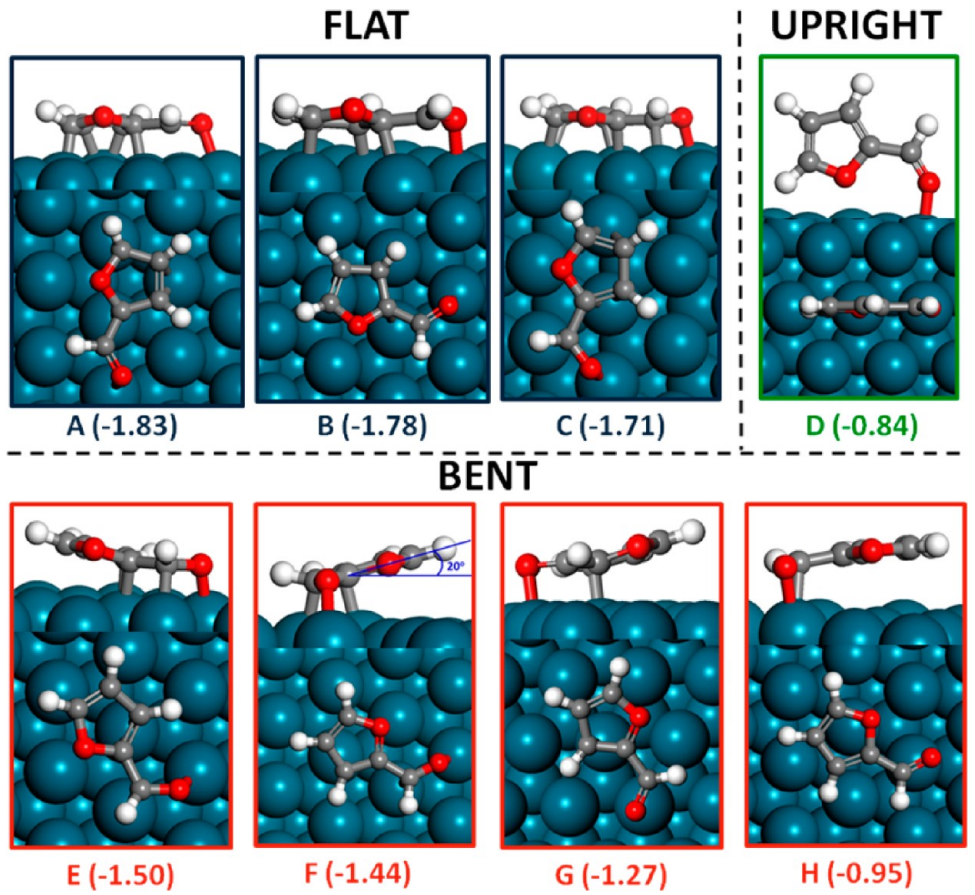

Figure 2. Furfural adsorption conformations on Pd(111). The numbers in parentheses represent the adsorption energies in eV. The stability trend is flat > bent > upright. For flat conformations, the ring centered over the fcc-hollow site is preferred (unit cell: 4 × 4).

convergence with respect to the *k*-mesh and the energy cutoff. For all unit cells, the adsorption energy deviated by no more than 0.02 eV. All transition states were located using the climbing nudged elastic band (cNEB) method.[35] We performed vibrational analysis to verify each of the reported transition states by locating a single imaginary frequency along the reaction coordinate. All of the lowest-energy conformations and intermediates were confirmed to have all real frequencies.

3. ADSORPTION OF FURANIC COMPOUNDS ON PD(111)

Here, we present the adsorption of key furanic compounds: furan, furfural, furfuryl alcohol, and 2-methylfuran on Pd(111). Furan is the simplest furanic compound, and its adsorption on Pd(111) has been studied using theory and experiments. Thus, we started with the PBE-D3 description of this system to validate the functional choice and to compare with experimental data. We optimized various structures of furan on Pd(111), similar to the DFT study of Woodruff and co-workers.[10] In addition, we searched for the most stable configuration at different coverages and tilt angles with respect to the surface. Three main surface arrangements were considered: (a) flat with the furan ring parallel to the surface, (b) bent with a furan ring tilted away from the surface, and (c) upright with the molecular plane perpendicular to the surface. Figure 1 shows how both coverage and orientation of the molecular plane affect the adsorption energies of the most stable geometries. At all coverages, the preferred adsorption configuration is a flat one with the ring centered over a hollow site and the oxygen located over the bridge site.

The two flat configurations shown in Figure 1 bind to either two or three Pd atoms. The one that binds to three Pd atoms is

dx.doi.org/10.1021/cs300395a | ACS Catal. 2012, 2, 2496−2504

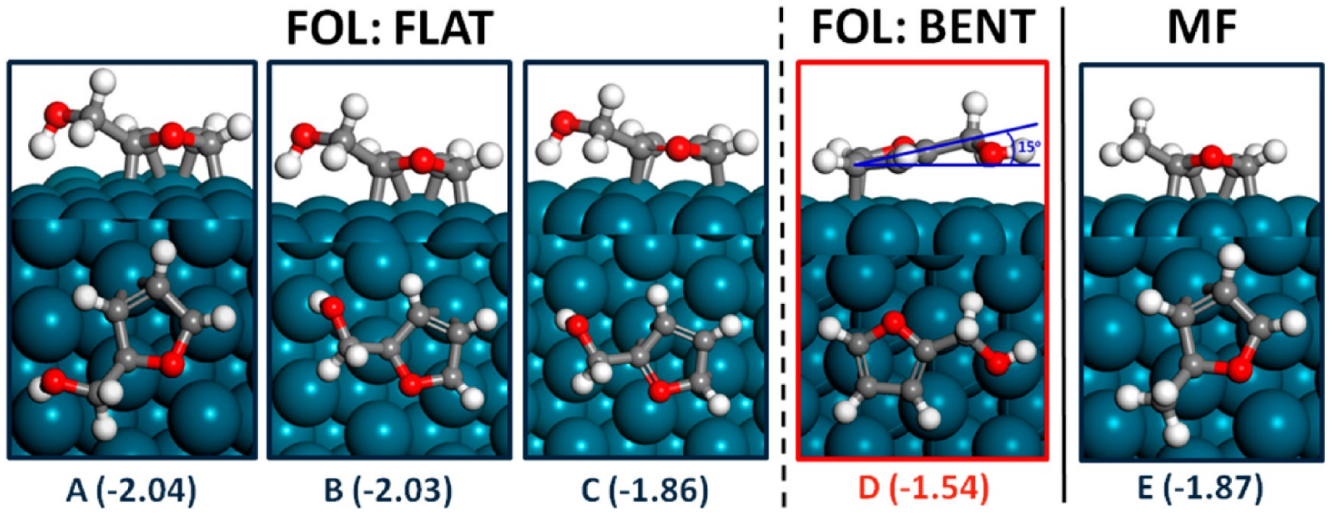

Figure 3. Furfuryl alcohol (FOL) and 2-methylfuran (MF) adsorption conformations on Pd(111). The numbers in parentheses represent the adsorption energies in eV. The most stable structure is with the furan ring centered over the fcc-hollow site and oxygen over the bridge site, similar to furan and furfural (unit cell: 4 × 4).

Table 2. Species Adsorption Energies on Pd(111) Computed via DFT Compared with TPD Adsorption Energies Obtained Using the Redhead Equation[a]

	conformation/unit cell size	DFT $\Delta E_{ads}/E_{disp}$ (eV)	exp. coverage	ΔE_{ads} TPD (eV)[13,20]
furan	flat/4 × 4	−1.58/−0.73	lowest	decomposes
	flat/3 × 3	−1.39/−0.73	low	−0.94 ± 0.19
	flat/2 × 2	−1.32/−1.14	high	−0.65 ± 0.13
furfural	flat/4 × 4	−1.83/−1.13	low	−0.98 ± 0.20
	bent/4 × 4	−1.50/−1.06		
	upright/4 × 4	−0.84/−0.68	high/multilayer	−0.65 ± 0.13
furfuryl alcohol	flat/4 × 4	−2.04/−1.16	low	decomposes
	bent/4 × 4	−1.54/−1.14	high/multilayer	−0.70 ± 0.14
2-methylfuran	flat/4 × 4	−1.87/−1.14		

[a] E_{disp} represents the computed van der Waals contribution to the adsorption energy.

preferred by 0.05 eV at low coverage and by 0.30 eV at high coverage. Other flat-lying structures considered (not shown here) either converged to one of the structures shown in Figure 1 or were displaced away from the Pd(111) surface entirely, resulting in weaker adsorption. The difference between hcp and fcc hollow sites was ∼0.02 eV, consistent with the findings of Woodruff and co-workers.[10]

The adsorption energy of the preferred configuration decreases with increasing coverage, as found by varying the unit cell size. The furan adsorption energy drops from −1.58 eV at low coverage (a 4 × 4 unit cell) to −1.32 eV at high coverage (a 2 × 2 unit cell). The DFT results are consistent with the experimental studies, which suggest that furan adsorbs flat to the surface at low coverage.[14,36] However, since the adsorption energy of the bent and the upright configurations is not a strong function of coverage, one may expect that these adsorption configurations are preferred at a high enough coverage. The evidence of such a tilt at high furan coverage (1.5 L) was observed in experiments.[20]

Table 1 summarizes the energetically preferred furan adsorption geometric parameters found using DFT and experiments. The interatomic distances are practically not affected by the functional choice, coverage, or the dispersion correction. The fact that the PBE-D3 calculations result in the same furan adsorption geometry is an interesting finding because the inclusion of vdW interactions in DFT calculations could significantly influence the adsorption structure as in the case of thiophene adsorption on Cu (see Supporting Information). The distances between Pd and the furan carbon atoms nearest to the oxygen ($d_{Pd-\alpha C}$) are in good agreement with the experimental data. In estimating the other parameters ($d_{Pd-\beta C}$ and d_{Pd-O}) from photoelectron diffraction experiments, Knight et al. assumed that furan atoms stay in the same molecular plane.[14] However, all DFT calculations show that hydrogen and oxygen atoms tilt out of the molecular plane away from the Pd surface, which is discussed in detail in Bradley et al.[10] As such, the comparison of $d_{Pd-\beta C}$ and d_{Pd-O} is less satisfactory.

Similarly to furan, we searched for the most stable flat, bent, and upright configurations of furfural, furfuryl alcohol, and 2-methylfuran. The flat configurations had all carbons of the furan ring bound to the surface. Bent structures were defined as those with only two furanic carbon atoms interacting with Pd(111), with the molecular plane tilted with respect to the surface, or as the carbonyl C or CO interacting with Pd(111) with the furan ring tilted away from the surface. The upright geometries were the ones with the furan ring completely perpendicular to the surface.

Figure 2 shows the adsorption conformers of furfural on the Pd(111) surface. There is a clear preference for furfural adsorption in flat conformation over the hollow site. The fcc and hcp hollow sites are close in energy (within 0.02 eV),

dx.doi.org/10.1021/cs300395a | ACS Catal. 2012, 2, 2496−2504

Table 3. Energetics for Furfural Reactions on Pd(111)[a]

reaction type	reaction	ΔE (eV)	E_{Af} (eV)	E_{Ab} (eV)
adsorption	$C_4H_3(CHO)O + * \rightarrow C_4H_3(CHO)O*$	−1.83		
	$C_4H_3(CH_2OH)O + * \rightarrow C_4H_3(CH_2OH)O*$	−2.04		
	$C_4H_4O + * \rightarrow C_4H_4O*$	−1.58		
	$C_4H_3(CH_3)O + * \rightarrow C_4H_3(CH_3)O*$	−1.87		
furan ring C−H scission	$C_4H_4O* + * \rightarrow C_4H_3O* + H*$	1.19 (1.46)	1.82 (1.82)	0.63 (0.36)
carbonyl C−H and O−H scission	$C_4H_3(CH_2OH)O* + * \rightarrow C_4H_3(CHOH)O* + H*$	−0.28 (0.07)	0.51 (0.51)	0.80 (0.44)
	$C_4H_3(CH_2OH)O* + * \rightarrow C_4H_3(CH_2O)O* + H*$	0.20 (0.38)	0.91 (0.91)	0.71 (0.53)
	$C_4H_3(CHOH)O* + * \rightarrow C_4H_3(CHO)O* + H*$	−0.27 (−0.03)	0.40 (0.40)	0.68 (0.44)
	$C_4H_3(CH_2O)O* + * \rightarrow C_4H_3(CHO)O* + H*$	−0.76 (−0.61)	0.34 (0.34)	1.10 (0.96)
	$C_4H_3(CHO)O* + * \rightarrow C_4H_3(CO)O* + H*$	0.23 (0.43)	0.95 (0.95)	0.72 (0.52)
	$C_4H_3(CHOH)O* + * \rightarrow C_4H_3(COH)O* + H*$	0.84 (0.88)	1.10 (1.10)	0.26 (0.22)
	$C_4H_3(COH)O* + * \rightarrow C_4H_3(CO)O* + H*$	−0.89 (−0.84)	0.19 (0.19)	1.07 (1.03)
C−C scission	$C_4H_3(CO)O* + * \rightarrow C_4H_3O* + CO*$	−0.49 (−0.42)	0.68 (0.68)	1.17 (1.09)
	$C_4H_3(CHO)O* + * \rightarrow C_4H_3O* + CHO*$	1.16		
	$C_4H_3(CH_2O)O* + * \rightarrow C_4H_3O* + CH_2O*$	1.22		
	$C_4H_3(COH)O* + * \rightarrow C_4H_3O* + COH*$	0.28 (0.43)	1.30 (1.30)	1.00 (0.87)
	$C_4H_3(CHOH)O* + * \rightarrow C_4H_3O* + CHOH*$	1.31		
	$C_4H_3(CH_2OH)O* + * \rightarrow C_4H_3O* + CH_2OH*$	1.60		
	$C_4H_3(C)O* + * \rightarrow C_4H_3O* + C*$	0.87 (0.99)	1.77 (1.77)	0.89 (0.74)
	$C_4H_3(CH)O* + * \rightarrow C_4H_3O* + CH*$	0.76 (0.88)	1.32 (1.32)	0.56 (0.44)
	$C_4H_3(CH_2)O* + * \rightarrow C_4H_3O* + CH_2*$	1.35		
	$C_4H_3(CH_3)O* + * \rightarrow C_4H_3O* + CH_3*$	1.96		
C−O scission	$C_4H_3(CH_2OH)O* + * \rightarrow C_4H_3(CH_2)O* + OH*$	0.06 (0.24)	1.05 (1.05)	0.99 (0.81)
	$C_4H_3(CH_2OH)O* + H* \rightarrow C_4H_3(CH_2)O* + H_2O*$	−0.21 (0.22)	0.85 (0.89)	1.06 (1.10)
	$C_4H_3(CHOH)O* + * \rightarrow C_4H_3(CH)O* + OH*$	0.88		
	$C_4H_3(CHOH)O* + H* \rightarrow C_4H_3(CH)O* + H_2O*$	0.61 (0.61)	1.33 (1.54)	0.72 (0.93)
	$C_4H_3(COH)O* + * \rightarrow C_4H_3(C)O* + OH*$	0.93		
	$C_4H_3(COH)O* + H* \rightarrow C_4H_3(C)O* + H_2O*$	0.64		
	$C_4H_3(CH_2O)O* + * \rightarrow C_4H_3(CH_2)O* + O*$	−0.25 (−0.17)	0.09 (0.09)	0.34 (0.25)
	$C_4H_3(CHO)O* + * \rightarrow C_4H_3(CH)* + O*$	1.02		
	$C_4H_3(CO)O* + * \rightarrow C_4H_3(C)* + O*$	1.11		
methyl C−H scission	$C_4H_3(CH)O* + * \rightarrow C_4H_3(C)O* + H*$	0.17		
	$C_4H_3(CH_2)O* + * \rightarrow C_4H_3(CH)O* + H*$	0.53		
	$C_4H_3(CH_3)O* + * \rightarrow C_4H_3(CH_2)O* + H*$	−0.01 (0.07)	0.62 (0.62)	0.63 (0.55)

[a] ΔE represents the reaction energy with respect to separate slabs. E_{Af}/E_{Ab} represents the forward/backward activation barriers. The numbers in parentheses are those computed with respect to same slabs (with co-adsorbates taken into account).

similar to results obtained for furan adsorption by Bradley et al.[10] and the ones reported here. The bent conformations have significant interaction with the surface through the carbonyl group but are less stable than the flat ones. Upright configurations are significantly less preferred relative to the flat and bent conformers. In addition, the trans isomer of furfural and furfuryl alcohol was found to be a slightly more favorable (by ∼0.1−0.2 eV) surface conformation.

The furfuryl alcohol and 2-methylfuran optimized configurations are presented in Figure 3. Again, the adsorption with the furan ring centered over the fcc-hollow site is the most favorable. There is 0.1 eV preference over other flat configurations and 0.5 eV preference over the bent ones. The upright configurations experience no significant binding, and thus, they are not included here. 2-Methylfuran adsorption with the ring over the fcc hollow site was preferred, with the methyl group tilted away from the molecular plane to preserve the sp^3 hybridization.

Table 2 compares DFT-computed binding energies with those obtained from TPD experimental data using the Redhead equation (ΔE_{ads} (eV) = $-0.0026T_{peak}/K \pm 20\%$).[37] The furan adsorption energy appears to be overestimated by the PBE-D3 treatment. However, as we show later, the surface reaction energies and barriers are not affected by the functional choice. It is also noteworthy that the TPD-derived value for furan adsorption in low coverage is −0.94 eV, whereas at even lower coverages (furan doses below 0.25 L), furan decomposes to H_2, CO, and C_xH_x species.[20] This means that an anticipated value for furan adsorption in very low coverages would be higher than −0.94 eV, closer to the DFT (PBE-D3) calculated one, −1.58 eV. Other potential reasons for the adsorption energy overestimation using PBE-D3 are the functional-inherent electrostatic interactions as described in the Methods section and the error in the vdW contribution.

Similar trends are seen for furfural and furfuryl alcohol desorption.[13] For furfural, the low-coverage TPD peak observed for molecular desorption occurs at a temperature of ∼375 K, corresponding to an −0.98 ± 0.20 eV adsorption energy. Furfuryl alcohol is speculated to desorb only from a liquid-like multilayer. The desorption peak at 270 K corresponds to an adsorption energy of −0.70 ± 0.14 eV. The rest of the furfuryl alcohol reacts to furfural, 2-methylfuran, and furan without any molecular desorption. This is likely why there is such a great difference between the TPD and DFT adsorption energies for furfuryl alcohol.

dx.doi.org/10.1021/cs300395a | ACS Catal. 2012, 2, 2496−2504

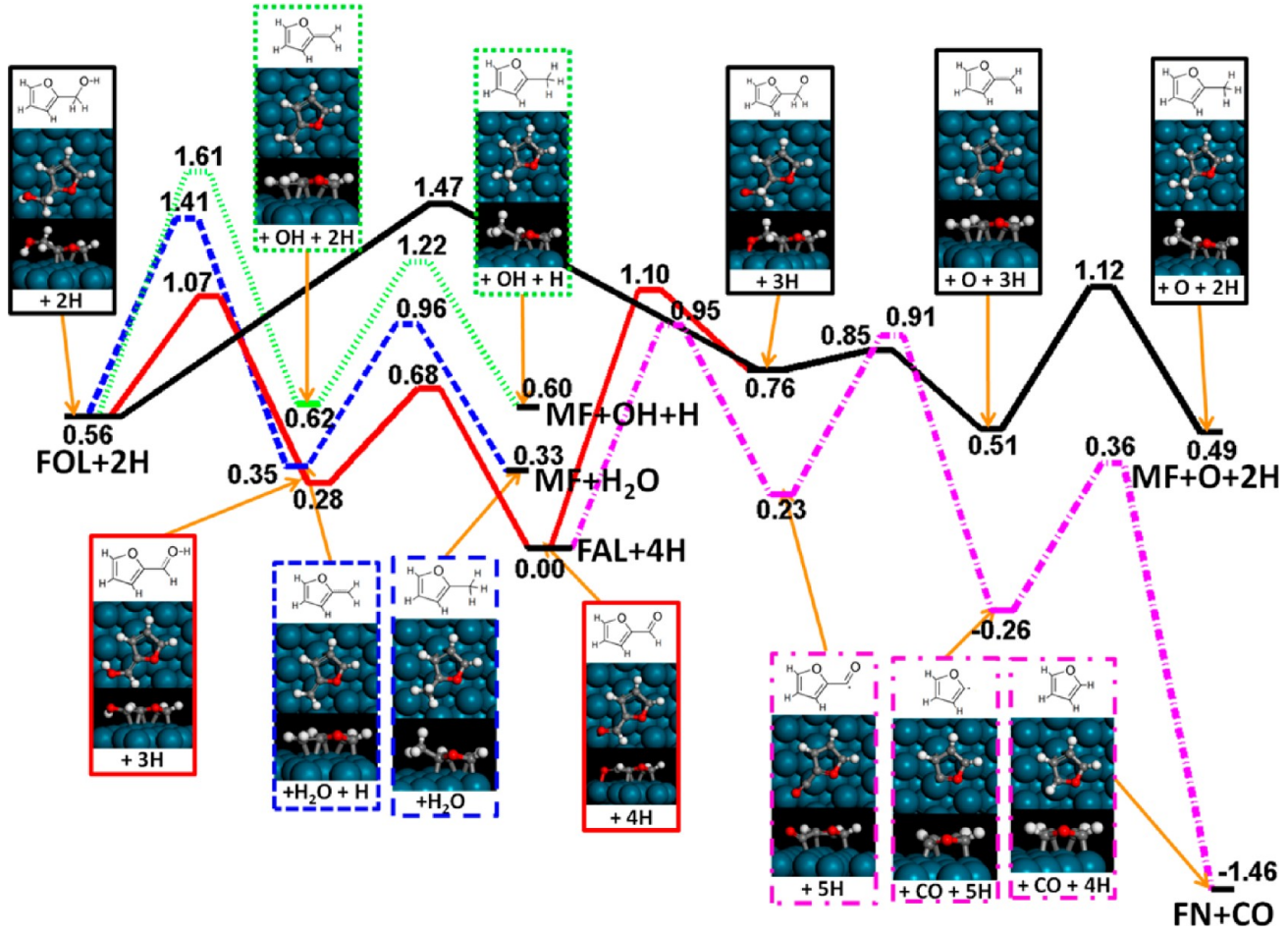

Figure 4. Potential energy diagram for surface reaction of furfural to furan, furfuryl alcohol, and 2-methylfuran. The energies (in eV) are with respect to furfural on Pd(111) plus four hydrogen atoms. The different reaction paths are (a) dehydroxylation of furfuryl alcohol (FOL) to 2-methylfuran (MF) (dotted green); (b) dehydration of FOL to MF (dashed blue); (c) dehydrogenation of FOL to a furylmethoxy intermediate, followed by its deoxygenation to MF (solid black); (d) dehydrogenation of furfural (FAL) to furan (FN) and CO (dash-dot magenta); and (e) dehydrogenation of FOL to FAL through a hydroxy intermediate and FAL hydrogenation to methoxy intermediate (solid red). The optimized structures of the intermediates are included.

4. FURFURAL REACTION TO FURAN, FURFURYL ALCOHOL AND 2-METHYFURAN

The initial results for the adsorption of the reactants and products (furan, furfural, furfuryl alcohol, and 2-methylfuran) showed that the energetically preferred configuration is the flat fcc-hollow-centered furan ring. We thus assume that all of the intermediates involved in the interconversion of these furanic compounds exhibit similar, flat binding conformation. For all of these intermediates, we started structural relaxations with the same furan ring placement over the fcc-hollow site.

We performed transition state search for (1) all of the hydrogenation/dehydrogenation reactions of the carbonyl and methyl substituent groups; (2) all of the C−C scission reactions between furyl carbon and the carbon of a substituent group; and (3) the C−O scission reactions of the $-CH_xO_y$ substituent groups, including deoxygenation, dehydroxylation, and hydrogen-assisted dehydroxylation. The few C−O scission reactions not reported here have high ΔE_{rxn} and, by Bronsted−Evans−Polanyi correlation estimates (not reported here), have barriers >1.5 eV and as such are not relevant to the chemistry investigated here. The reaction energies with their corresponding activation barriers are given in Table 3. All of the surface reactions are in the decomposition direction, starting with a single adsorbate initial state. This is why most of the reactions have the same forward activation barrier, irrespective of using separate- or same-slab references. The most likely paths for the described reactions are presented in Figure 4. All of the intermediates are referenced to separate slabs. This methodology[38−40] has been extensively used in the literature. We used the highest barriers along the specified paths in Figure 4 to infer the dominant pathways.

It is worth mentioning that the reaction energies for furfural and furfuryl alcohol reactions to furan and 2-methylfruan reported by Pang and Medlin are almost identical to those found here (this comparison may be found in the Supporting Information).[13] Pang and Medlin used the PW-91 functional, which performs similarly to the PBE functional. This indicates that while the dispersion forces affect the binding energies (shown earlier), their energetic component to the reaction energies and barriers is minimal.

From Table 3 and Figure 4, we see that the formation of furan and CO from furfural is thermodynamically favored. In Figure 4, furan is found at the lowest potential energy. In Table 3, the most exothermic reactions are for furfural decomposition to furan. In ultrahigh vacuum experiments, furfural decarbonylation to furan is, indeed, preferred on Pd, especially with no

dx.doi.org/10.1021/cs300395a | ACS Catal. 2012, 2, 2496−2504

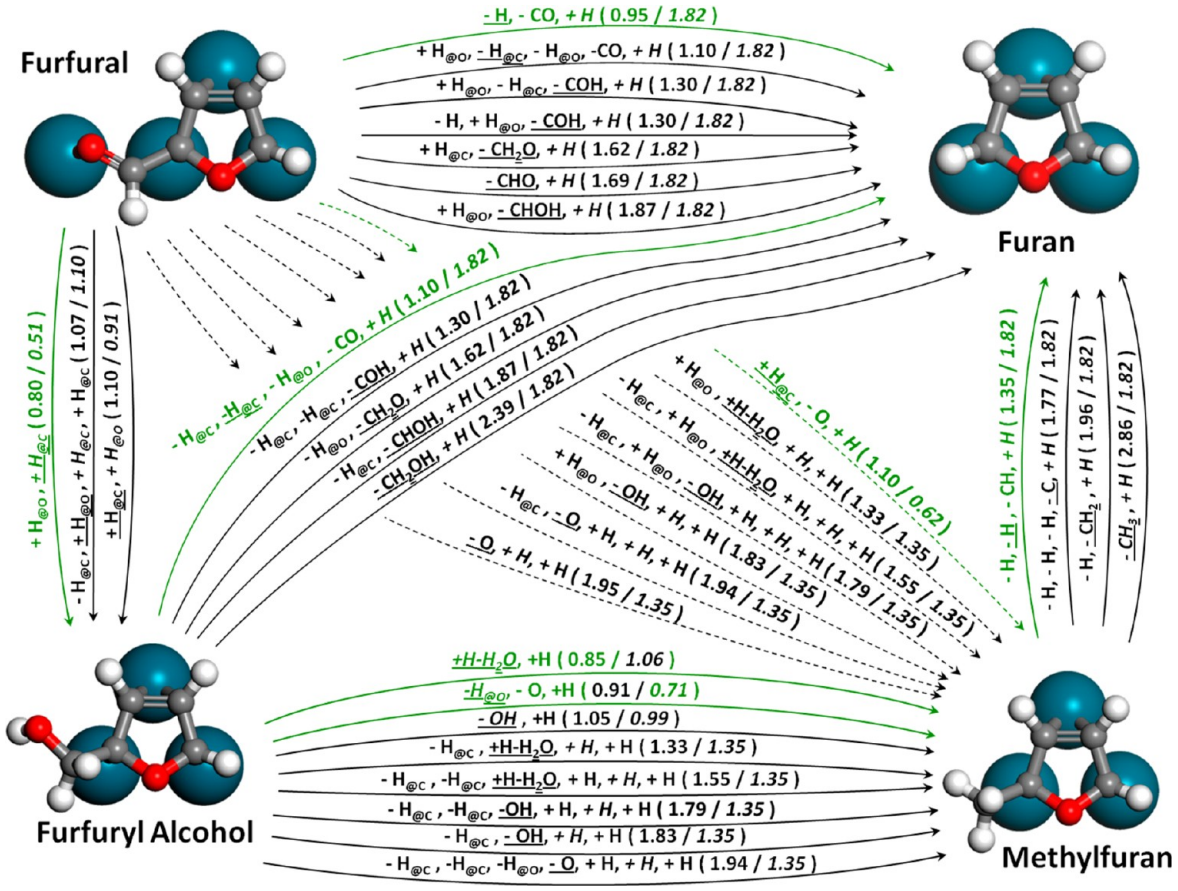

Figure 5. Pathways for the interconversion of furfural, furfuryl alcohol, furan, and 2-methylfuran. Each arrow corresponds to a distinct set of elementary reactions, keeping the furyl ring unaltered. The reactions with highest barriers along each path are underlined and italicized for the forward and backward paths, respectively. The corresponding highest barriers, in eV, along each path are given as (forward path/*backward path*). The most preferred paths between each of the surface species are highlighted in green.

hydrogen cofeed;[13] however, this picture becomes more complicated when kinetic barriers are considered. Figure 5 shows a summary of potential pathways for the interconversion of furfural, furfuryl alcohol, furan, and 2-methylfuran. It reveals the most preferred paths while also establishing the possibility for direct pathways between the main surface species.

Furfural may undergo dehydrogenation, decarbonylation, and subsequent hydrogenation with the highest barrier of 0.95 eV to form furan. In addition to this energetically most preferred path, an energetically close path exists where furfural undergoes a series of hydrogenation/dehydrogenation and decarbonylation reactions to form furan (highest barrier of 1.10 eV). The reverse reactions of converting furan to furfural are unfavorable.

The preferred pathway for furfural hydrogenation to furfuryl alcohol occurs first via hydrogenation of the carbonyl oxygen followed by the hydrogenation of the carbon and has the highest barrier of 0.80 eV in the last hydrogenation step of converting $-CHOH$ to $-CH_2OH$ (see the solid red line in Figure 4). This is consistent with previous studies of this reaction on both copper and palladium.[9,13] The hydrogenation at the carbon first followed by the hydrogenation of the oxygen is less preferred, with the highest barrier of 1.10 eV. An additional path through an acyl intermediate ($C_4H_3(CO)O^*$) involves more steps, but has a highest barrier of 1.07 eV. It is clear that at higher temperatures, multiple parallel pathways exist (redundancy) in converting furfural to furfuryl alcohol because all of the paths have highest barriers of ∼1 eV.

The relatively low reaction barriers (0.68, 0.80 eV) of furfural conversion to furfuryl alcohol imply that some furfuryl alcohol can be produced in kinetic experiments, and the ratio of products should depend on the hydrogen coverage and, thus, on the hydrogen partial pressure and temperature. In vapor phase experiments, furfural has been found to convert to both furan and furfuryl alcohol in a 4:1 ratio under certain conditions.[4]

Furfural can undergo direct hydrodeoxygenation to yield 2-methylfuran, bypassing furfuryl alcohol as an intermediate. This route has the highest barrier of 1.10 eV associated with initial hydrogenation of the carbon of the substituent group. However, the most preferred path from furfural leading to 2-methylfuran lies through furfuryl alcohol.

Starting from furfuryl alcohol, one can produce furan, furfural, or 2-methylfuran. Furfuryl alcohol may undergo direct decomposition to furan, with the highest barrier being 1.10 eV associated with C−H cleaving. Alternatively and more preferably, it will first dehydrogenate to furfural, followed by furfural decarbonylation, as previously discussed. The initial and highest kinetic barrier for the dehydrogenation of furfuryl alcohol to furfural is only 0.51 eV. This dehydrogenation barrier is ∼0.34 eV lower than the highest barrier in the production of 2-methylfuran, as discussed below. This is consistent with the experiments, in which most of furfuryl alcohol decomposes to

dx.doi.org/10.1021/cs300395a | *ACS Catal.* 2012, 2, 2496−2504

furfural and furan, with some 2-methylfuran also observed.[13] It is noteworthy that our DFT calculations are representative of a low hydrogen surface coverage. The increase in the surface hydrogen coverage may cause site blocking for furfuryl alcohol dehydrogenation and, thus, result in a higher probability of dehydration.

The formation of the hydroxyalkyl intermediate in furfuryl alcohol dehydrogenation (alcohol C−H scission first, followed by O−H scission second) is more favored, according to our DFT calculations. This is consistent with several of the latest DFT calculations.[9,13,41,42] On the other hand, Barteau and co-workers have concluded that alcohol oxidation occurs via O−H scission first.[43,44] Because of small differences in energetics computed in this work, both pathways may be relevant under reaction conditions. It is possible that this pathway is metal-specific and that it is oxygen-coverage-dependent. In addition, steric effects may play a role in why C−H scission is favored in alcohol oxidation. Specifically, all of our calculations were performed in the limit of low coverage. When multiple coadsorbates are considered, the adsorption through carbon may be harder, in which case O−H scission may be favored because it is the end group of the molecule. The effect of surface coverage will also be worth investigating in future work.

The hydrodeoxygenation of furfuryl alcohol to 2-methylfuran can occur via dehydroxylation followed by hydrogenation or via hydrogen-assisted dehydroxylation followed by hydrogenation, which is also depicted in Figure 4 (dashed blue and dotted green lines, respectively). The C−O bond-breaking has the highest barrier in each of these two reactions. The furfuryl alcohol dehydration barrier (0.85 eV via H-assisted OH removal; dashed blue line) is 0.2 eV lower than the barrier for direct dehydroxylation (1.05 eV; dotted green line). There is another deoxygenation pathway leading to 2-methylfuran, for which the highest barrier is 0.91 eV for the initial O−H bond breaking (solid black line in Figure 4). In this path, furfuryl alcohol first dehydrogenates to a methoxy intermediate ($C_4H_3(CH_2O)O^*$). The methoxy intermediate directly deoxygenates with a low activation barrier of 0.09 eV, likely because the oxygen is activated through its interaction with the surface. In addition, this is the only exothermic C−O cleaving reaction when considering coadsorbate effects in the final state ($C_4H_3(CH_2)O^* + O^*$), as seen in Table 3, further explaining a low barrier. 2-Methylfuran is then formed via a low barrier (~0.63 eV) hydrogenation. The energetics indicates that all three pathways may be relevant under reaction conditions, and the preference of each pathway may also depend on the hydrogen coverage. In addition, coverage effects from any coadsorbates (e.g., hydrogen in hydrogenation, oxygen in oxidation, spectators forming in the catalytic cycle, and the main reagent such as furfural) are often important and need to be accounted for as corrections in rate constants during the development of microkinetic models.[45,46]

The reactions of 2-methylfuran to furfural and furfuryl alcohol are more interesting. 2-Methylfuran has low barriers for its oxygenation directly to furfural or furfuryl alcohol. The highest barrier along the preferred path to furfural is 0.62 eV, whereas the one to furfuryl alcohol is 0.71 eV. This may explain why only a small amount of 2-methylfuran is observed in TPD experiments and why no 2-methylfuran formation is observed in continuous flow reactor experiments. Furan is the only species not likely to form directly from 2-methylfuran because the highest barrier for the preferred path is 1.35 eV.

The preferred paths for furfural, furfuryl alcohol, or 2-methylfuran conversion to furan go through an acyl intermediate ($C_4H_3(CO)O^*$). C−C cleaving of the acyl intermediate is the only exothermic C−C scission reaction and has a low barrier of 0.68 eV. Following the C−C cleaving, the furyl intermediate ($C_4H_3O^*$) can be easily hydrogenated with a low barrier of 0.63 eV. The next-lowest C−C scission barriers are 1.30 and 1.32 eV for $C_4H_3(COH)O^*$ and $C_4H_3(CH)O^*$ C−C scission, respectively, and are higher than the acyl intermediate C−C scission by more than 0.60 eV. Other $C_{furyl}-CH_xO_y$ C−C scission reactions have higher (>1 eV) reaction energies and will thus have even higher barriers. As a result, it is more likely that furfural or furfuryl alcohol undergo dehydrogenation to acyl intermediate prior to C−C scission.

Even with availability of H, O, and CH_xOH_y species on the surface, the conversion of furan to any other surface species is limited by the initial dehydrogenation of the α-carbon, with a barrier of 1.82 eV. This implies that furan likely is not an intermediate in any of the hydrogenation/dehydrogenation reactions of furfural or furfuryl alcohol.

5. CONCLUSIONS

We performed detailed density functional theory (DFT) calculations on the adsorption configurations and reaction energetics of furfural conversion to furan, furfuryl alcohol, and 2-methylfuran on Pd(111) using the dispersion-corrected PBE-D3 functional. For all—furan, furfural, furfuryl alcohol, and 2-methylfuran—the most stable conformation was with the furan ring lying flat on the surface, centered over a hollow site.

Furfural reaction thermodynamics clearly favors the production of furan and CO. The DFT results show that the apparent reaction barrier for furfural decomposition to furan is 0.15 eV higher than that for furfural reaction to furfuryl alcohol. This explains the experimental observations in furfural hydrogenation.[13] Mechanistically, the furfural transformation to furfuryl alcohol occurs via hydrogenation of the carbonyl oxygen first. The furfuryl alcohol reaction to 2-methylfuran occurs through hydrogen-assisted dehydration (hydrogen-assisted OH removal) rather than dehydroxylation with an activation barrier 0.2 eV lower. Another competitive path for 2-methylfuran production involves dehydrogenation to a methoxy intermediate, followed by low-barrier (0.09 eV) deoxygenation. Our findings are consistent with a series of experimental observations regarding the adsorption and reaction of furfural and furfuryl alcohol on Pd(111). For example, recent TPD studies showed that furfural and furfuryl alcohol undergo decarbonylation to furan and CO, which is consistent with both our calculated thermodynamics and reaction barriers.[13] In addition, the relatively small kinetic barriers for furfural and furfuryl alcohol hydrogenation found in this study are consistent with observing hydrogenation products in the supported catalyst studies.[4,7]

■ ASSOCIATED CONTENT

Ⓢ Supporting Information

Additional Information as noted in text. This material is available free of charge via the Internet at http://pubs.acs.org.

■ AUTHOR INFORMATION

Corresponding Author

*Phone: 302-831-2830. E-mail: vlachos@udel.edu.

Author Contributions

†V.V. performed all calculations. D.G.V. conceptualized the study, and D.G.V. and G.M. carried out the advising and improved the paper writing.

Notes

The authors declare no competing financial interest.

■ ACKNOWLEDGMENTS

V.V. performed all calculations. D.G.V. conceptualized the study, and D.G.V. and G.M. carried out the advising and improved the paper writing. V.V. acknowledges support from an NSF graduate fellowship. V.V.'s and D.G.V.'s work is supported in part by an NSF-CDI I Grant (CBET-940768). G.M.'s work is based upon work financially supported as part of the Catalysis Center for Energy Innovation, an Energy Frontier Research Center funded by the U.S. Department of Energy, Office of Science, Office of Basic Energy Sciences under Award No. DE-SC0001004. DFT calculations were performed using the TeraGrid resources provided by Texas Advanced Computing Center (TACC) of the University of Texas at Austin.

■ REFERENCES

(1) Werpy, T.; Petersen, G. *Top Value Added Chemicals from Biomass: Volume I — Results of Screening for Potential Candidates from Sugars and Synthesis Gas*; National Renewable Energy Laboratory (NREL): Golden, CO, 2004, pp 1–27.
(2) Lange, J.-P.; van der Heide, E.; van Buijtenen, J.; Price, R. *ChemSusChem* **2012**, *5* (1), 150–166.
(3) Dutta, S.; De, S.; Saha, B.; Alam, M. I. *Cataly. Sci. Technol.* **2012**, *2* (10), 2025–2036.
(4) Sitthisa, S.; Resasco, D. *Catal. Lett.* **2011**, *141* (6), 784–791.
(5) Kaufmann, W. E.; Adams, R. *J. Am. Chem. Soc.* **1923**, *45* (12), 3029–3044.
(6) Burnett, L. W.; Johns, I. B.; Holdren, R. F.; Hixon, R. M. *Ind. Eng. Chem.* **1948**, *40* (3), 502–505.
(7) Sitthisa, S.; Pham, T.; Prasomsri, T.; Sooknoi, T.; Mallinson, R. G.; Resasco, D. E. *J. Catal.* **2011**, *280* (1), 17–27.
(8) Rao, R.; Baker, R.; Vannice, M. *Catal. Lett.* **1999**, *60* (1), 51–57.
(9) Sitthisa, S.; Sooknoi, T.; Ma, Y.; Balbuena, P. B.; Resasco, D. E. *J. Catal.* **2011**, *277* (1), 1–13.
(10) Bradley, M. K.; Robinson, J.; Woodruff, D. P. *Surf. Sci.* **2010**, *604* (11–12), 920–925.
(11) Bradley, M. K.; Duncan, D. A.; Robinson, J.; Woodruff, D. P. *Phys. Chem. Chem. Phys.* **2011**, *13* (17), 7975–7984.
(12) Sitthisa, S.; An, W.; Resasco, D. E. *J. Catal.* **2011**, *284* (1), 90–101.
(13) Pang, S. H.; Medlin, J. W. *ACS Catal.* **2011**, 1272–1283.
(14) Knight, M. J.; Allegretti, F.; Kröger, E. A.; Polcik, M.; Lamont, C. L. A.; Woodruff, D. P. *Surf. Sci.* **2008**, *602* (14), 2524–2531.
(15) Rohlfing, M.; Bredow, T. *Phys. Rev. Lett.* **2008**, *101*, 26.
(16) Mpourmpakis, G.; Froudakis, G. E. *J. Nanosci. Nanotechnol.* **2008**, *8* (6), 3091–3096.
(17) Tonigold, K.; Gross, A. *J. Chem. Phys.* **2010**, *132* (22), 1–10.
(18) Jenkins, S. J. *Proc. R. Soc. A* **2009**, *465* (2110), 2949–2976.
(19) Kelkkanen, A.; Lundqvist, B. I.; Norskov, J. K. *Phys. Rev. B* **2011**, *83* (11), 113401.
(20) Ormerod, R. M.; Baddeley, C. J.; Hardacre, C.; Lambert, R. M. *Surf. Sci.* **1996**, *360* (1–3), 1–9.
(21) Sony, P.; Puschnig, P.; Nabok, D.; Ambrosch-Draxl, C. *Phys. Rev. Lett.* **2007**, *99* (17), 176401.
(22) Kresse, G.; Furthmüller, J. *Comput. Mater. Sci.* **1996**, *6*, 15.
(23) Kresse, G.; Furthmüller, J. *Phys. Rev. B* **1996**, *54*, 11169.
(24) Perdew, J. P.; Burke, K.; Ernzerhof, M. *Phys. Rev. Lett.* **1996**, *77*, 3865.
(25) Grimme, S.; Antony, J.; Ehrlich, S.; Krieg, H. *J. Chem. Phys.* **2010**, *132*, 15.
(26) Blöchl, P. E. *Phys. Rev. B* **1994**, *50*, 17953.
(27) Kresse, G.; Joubert, D. *Phys. Rev. B* **1999**, *59*, 1758.
(28) Monkhorst, H. J.; Pack, J. D. *Phys. Rev. B* **1976**, *13* (12), 5188–5192.
(29) Blochl, P. E.; Jepsen, O.; Andersen, O. K. *Phys. Rev. B* **1994**, *49* (23), 16223–16233.
(30) Murnaghan, F. D. *Proc. Natl. Acad. Sci. U.S.A.* **1944**, *30*, 244–247.
(31) Birch, F. *Phys. Rev.* **1947**, *71* (11), 809–824.
(32) Lamber, R.; Wetjen, S.; Jaeger, N. I. *Phys. Rev. B* **1995**, *51* (16), 10968–10971.
(33) Patnaik, G.; Kailasanath, K.; Oran, E. S. *AIAA J.* **1991**, *29*, 2141–2148.
(34) Pulay, P. *Chem. Phys. Lett.* **1980**, *73* (2), 393–398.
(35) Henkelman, G.; Uberuaga, B. P.; Jonsson, H. *J. Chem. Phys.* **2000**, *113* (22), 9901–9904.
(36) Futaba, D. N.; Chiang, S. *J. Vac. Sci. Technol., A* **1997**, *15* (3), 1295–1298.
(37) Masel, R. I. *Principles of Adsorption and Reaction on Solid Surfaces*; Wiley: New York, 1996.
(38) Salciccioli, M.; Vlachos, D. G. *ACS Catal.* **2011**, *1* (10), 1246–1256.
(39) Salciccioli, M.; Stamatakis, M.; Caratzoulas, S.; Vlachos, D. G. *Chem. Eng. Sci.* **2011**, *66* (19), 4319–4355.
(40) Ford, D. C.; Nilekar, A. U.; Xu, Y.; Mavrikakis, M. *Surf. Sci.* **2010**, *604* (19–20), 1565–1575.
(41) Jiang, R.; Guo, W.; Li, M.; Fu, D.; Shan, H. *J. Phys. Chem. C* **2009**, *113* (10), 4188–4197.
(42) Li, M.; Guo, W.; Jiang, R.; Zhao, L.; Shan, H. *Langmuir* **2009**, *26* (3), 1879–1888.
(43) Davis, J. L.; Barteau, M. A. *Surf. Sci.* **1987**, *187* (2–3), 387–406.
(44) Davis, J. L.; Barteau, M. A. *Surf. Sci.* **1990**, *235* (2–3), 235–248.
(45) Mhadeshwar, A. B.; Kitchin, J. R.; Barteau, M. A.; Vlachos, D. G. *Catal. Lett.* **2004**, *96* (1–2), 13–22.
(46) Salciccioli, M.; Stamatakis, M.; Caratzoulas, S.; Vlachos, D. G. *Chem. Eng. Sci.* **2011**, *66*, 4319–4355.